ACS APPLIED BIO MATERIALS

Article

Cite This: ACS Appl. Bio Mater. 2020, 3, 477−485

www.acsabm.org

Formation of a Au/Au_9Ga_4 Alloy Nanoshell on a Bacterial Surface through Galvanic Displacement Reaction for High-Contrast Imaging

Amanpreet Singh,[†] Deepak Bains,[‡] Walid M. Hassen,[†] Narinder Singh,*[,‡] and Jan J. Dubowski*[,†]

[†]Laboratory for Quantum Semiconductors and Photon-Based BioNanotechnology, Interdisciplinary Institute for Technological Innovation (3IT), CNRS UMI-3463, Department of Electrical and Computer Engineering, Université de Sherbrooke, 3000 boul. de l'Université, Sherbrooke, Québec J1K 0A5, Canada

[‡]Department of Chemistry, Indian Institute of Technology Ropar, Punjab 140001, India

Supporting Information

ABSTRACT: The spontaneous electron transfer between GaAs and ionic gold through the galvanic displacement reaction results in the formation of gold nanoparticles and a Au_9Ga_4 alloy. We investigated this process for decorating *Legionella pneumophila* and *Escherichia coli*, aiming at enhanced imaging of these bacteria. The surface of bacteria was modified with gold ions through the electrostatic linkage of ionic liquids with phosphate units of the bacterial cell wall. The modified bacteria were further incubated with an antibody-functionalized GaAs substrate. Due to a large gap in the reduction potential of gold and gallium ions, the induced reaction involving bacteria resulted in a reduction of the gold ions to gold nanoparticles and oxidation of GaAs to Ga_2O_3 and a Au_9Ga_4 alloy. The bacteria covered with a Au/AuGa nanoshell, if excited at 377 nm, show a bright emission at 447 nm originating from Au/Au_9Ga_4. This approach offers a simple and potentially less expensive method for high-contrast imaging of bacteria in comparison to the conventional methods of staining with different dyes or by conjugating green fluorescent proteins.

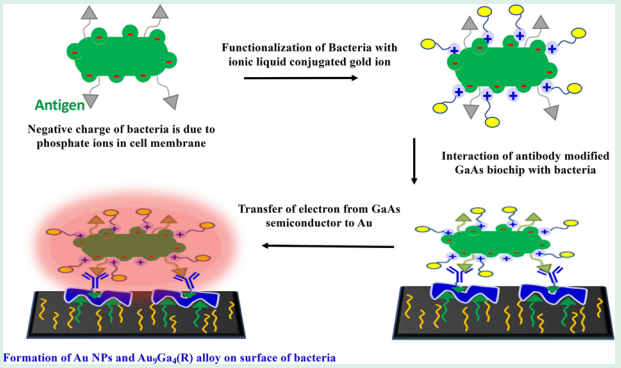

KEYWORDS: *galvanic displacement reaction, ionic liquids, GaAs, Au_9Ga_4 alloy, Legionella pneumophila, Escherichia coli, high-contrast imaging*

INTRODUCTION

The global spread of bacterial infections is a major health concern, and therefore, super-resolution imaging and proper diagnosis of bacteria are a priority for universal microbiology research.[1−5] For imaging purposes, bacterial research is sustained with some relatively expensive and time-consuming applications of fluorescent dyes or conjugation with green fluorescence proteins. There is a strong interest in finding alternative methods of imaging different strains of bacteria rapidly and at a low cost. Recently, some Forster resonance energy transfer (FRET) based molecular probes were reported for imaging of bacteria. For example, Chan et al. have conjugated a well-known Cephalosporin antimicrobial drug with two different fluorophores.[6] Binding of such a drug with the bacterial cell wall resulted in deposition of fluorescent probes on the surface of bacteria. Consequently, due to energy transfer between the acceptor and donor fluorophore, fluorescence intensity was significantly enhanced. Similarly, Liu et al. have developed a series of tetraphenylethene (TPE) based aggregation-induced emission (AIE) active receptors for effective bacteria imaging and discrimination.[7] These fluorogens enhance their fluorescence upon aggregation triggered due to restriction of intramolecular rotations. Therefore, upon interaction with the bacterial cell wall, the fluorescence intensity of TPE receptors significantly increases, which was further used for imaging and selective discrimination. However, tedious organic steps are required for synthesis of such organic probes. Comparatively, the fabrication of metallic nanoparticles on the surface of bacteria for imaging purposes would be easy and less expensive.[8]

Decorating the bacterial surface with metallic nanoparticles has gained growing interest driven by applications in catalysis[9] and sensing.[10−13] In this context, the formation of metallic nanoparticles by the galvanic displacement reaction (GDR) is attractive due to achievable uniform distributions of nanoparticles.[14−18] The GDR approach allows for electroless deposition of metal on the surface of semiconductors.[19−22] Different metallic ions tend to form core−shell nanomaterials.[23−25] The metallic ions with redox potential more positive than the substrate spontaneously accept electrons from the semiconductor lattice, and consequently, the reduced metal could be deposited on the surface of the substrate.[26,27]

Received: October 8, 2019
Accepted: December 11, 2019
Published: December 11, 2019

DOI: 10.1021/acsabm.9b00932
ACS Appl. Bio Mater. 2020, 3, 477−485

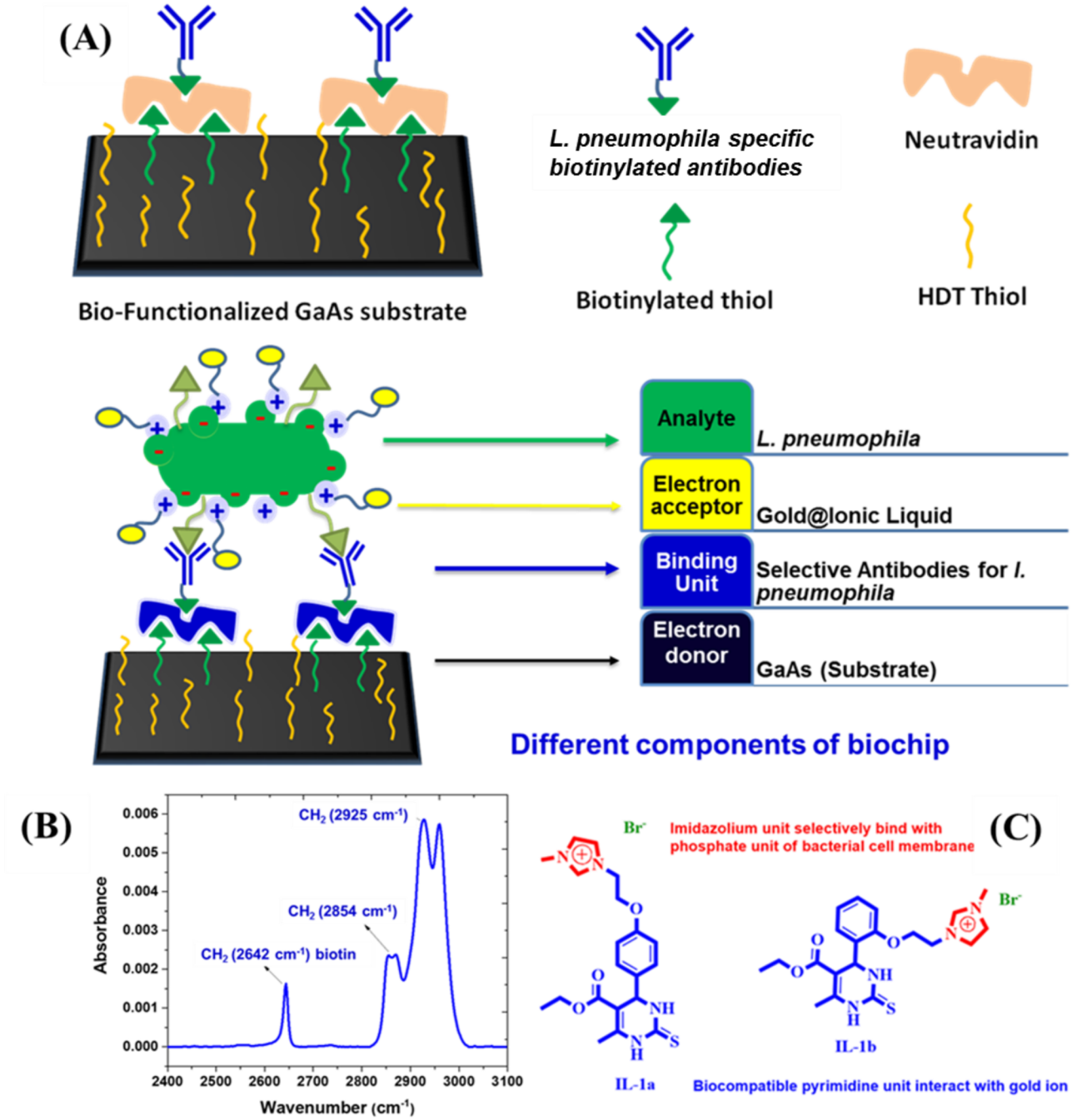

Figure 1. (a) Schematic representation of the biochip components. (b) FTIR spectra of the GaAs surface functionalized with HDT thiol and PEG-biotinlayted thiol. (c) Structure of ionic liquids used for decoration of bacteria.

We are focused on the biosensing research of *Escherichia coli*[28,29] and, particularly, *Legionella pneumophila*[30−33] because of the high risk of these bacteria to cause serious Legionnaires and Pontiac fever diseases.[34,35] In the past decade, more than 500 cases of Legionnaire's disease outbreaks were reported in Europe and North America with high mortality rates.[36] The objective of this work was to investigate the functionalization of bacterial cell walls with gold ions through linkage of ionic liquids[37−44] and, further, specifically immobilize decorated bacteria on antibody-functionalized GaAs biochips. The ionic liquid linkage inspires the binding of the gold ion with a phosphate unit of the bacterial cell wall.[45,46] During the immobilization, the galvanic displacement reaction takes place between GaAs and Au^{3+} ions. Consequently, a thin layer of Au nanoparticles and gold gallium (Au_9Ga_4) alloy forms on the surface of bacteria, giving a strong emission at 447 nm upon excitation at 377 nm. Using this approach, high contrast imaging of bacteria is obtained under a DAP filter of a fluorescence microscope.

RESULTS AND DISCUSSION

A schematic illustration of the investigated biochip structure is shown in Figure 1a. It consists of a GaAs substrate functionalized with biotinylated thiols, neutravidin, and biotinylated antibodies. The Au nanoparticle decorated bacteria have been achieved through the reaction of an ionic

DOI: 10.1021/acsabm.9b00932
ACS Appl. Bio Mater. 2020, 3, 477−485

Scheme 1. Synthetic Scheme of the Synthesis of Ionic Liquids

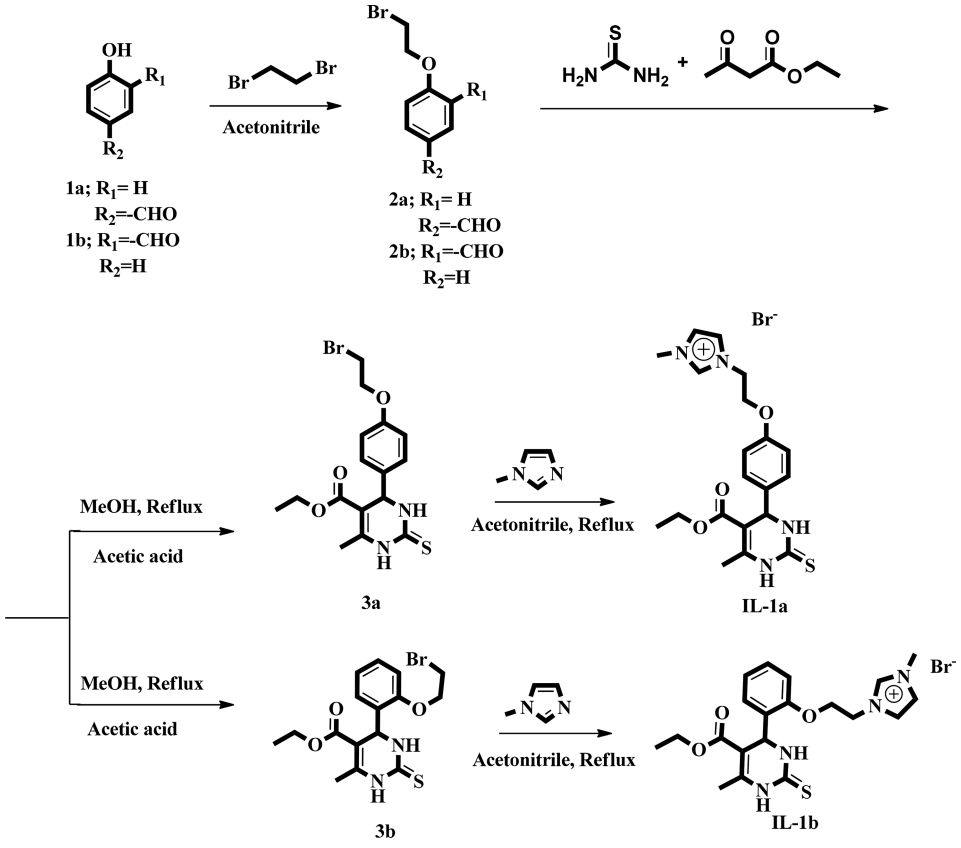

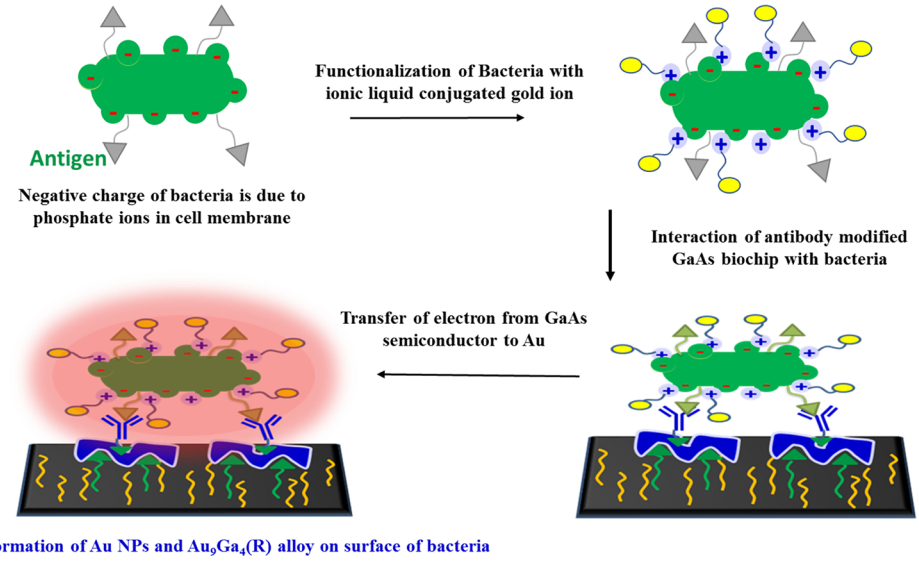

Figure 2. Schematic representation of the mechanisms of decoration of bacteria with Au nanoparticles.

liquid (IL) comprising Au^{3+} ions with a bacterial surface. We designed the IL in such a way that an imidazolium cation binding unit[47−50] binds with a phosphate ion in the cell membrane, and another side (thiourea linkage) interacts with a gold ion.[51,52] In this way, the Au^{3+} ions will only interact with the phosphate unit rather than the entire antigen. Scheme 1 provides details for the synthesis of ionic liquids.

Functionalization of the GaAs surface using alkaline thiols has been well established, and it has been employed to grafting bioreceptors, such as antibodies for selective capturing of target analytes, and consequently observe changes in photophysical properties of GaAs.[53−56] The 2 mm × 2 mm chips of GaAs (001) were washed with acetone, OptiClear, acetone, and isopropanol, respectively, followed by etching with an ammonium hydroxide solution to remove surface oxides. Further, the chips were exposed to a mixture of HDT thiol and PEG-biotinylated thiol (15:1, M/M). The formation of a mixed SAM structure was characterized using FTIR spectroscopy as illustrated in Figure 1b. The absorbance peaks at ∼2854 and ∼2925 cm^{-1}, corresponding to symmetric (ν_{sym})

DOI: 10.1021/acsabm.9b00932
ACS Appl. Bio Mater. 2020, 3, 477−485

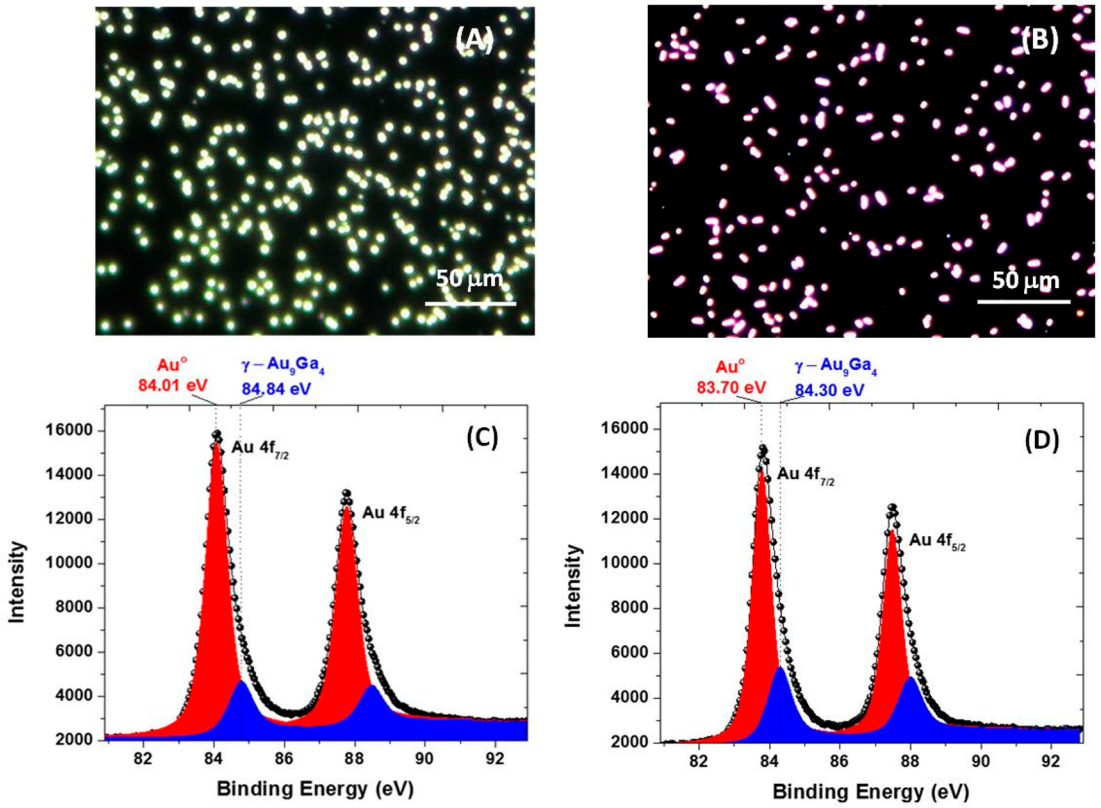

Figure 3. (a) Optical microscopy image of gold nanoparticles developed on the GaAs substrate through galvanic displacement reaction. (b) Optical microscopy image of a nanoshell of metallic gold revealing the surface of *E. coli* bacteria on a biofunctionalized substrate. (c) High-resolution XPS scans of the Au 4f peak from GaAs functionalized with gold ions (100 μM, exposed for 10 min). (d) High-resolution XPS scans of the Au 4f peak from biofunctionalized GaAs exposed to gold-coated bacteria.

and asymmetric (ν_{asym}) stretch vibrations of C−H bonds, revealed the presence of a well-organized SAM. The splitting of both ν_{sym} and ν_{asym} is consistent with the formation of a mixed SAM.[55] Afterward, the thiol-functionalized biochips were exposed, sequentially, to neutravidin and biotinylated antibodies. The structure of ionic liquids used for decoration of bacteria is shown in Figure 1c.

Decoration of Bacteria. Figure 2 describes the employed procedure for the decoration of bacteria with Au nanoparticles, as well as immobilization of the modified bacteria on the surface of GaAs. The phosphate unit of the bacterial cell membrane in Gram-negative bacteria induced the negative charge on its surface, which leads to a well-known interaction with positively charged imidazolium ionic liquids.[46,57,58] Thus, we synthesized the organic cations by conjugating the imidazolium unit with pyrimidine-based biocompatible receptors. The bromo-alkyl-substituted pyrimidine receptors were synthesized using the multicomponent Biginelli reaction[59] between aldehyde, thiourea, and ethyl acetoacetate by refluxing in acetonitrile using zinc perchlorate as a catalyst. Further, the product was purified using column chromatography and reacted with *N*-methyl imidazole. The resulting Biginelli receptors have two binding units: a positively charged cation for the phosphate ion and a thiourea subgroup for gold conjugation. Scheme 1 provides details for the synthesis of ionic liquids. The bacteria were first incubated in the aqueous solution of compound **IL-1a**, followed by the incubation in 200 μL of 10 mM solution of gold chloride. After 1 h incubation, the bacteria were separated out by centrifugation, and extra gold was removed. The zeta potential measurements of the functionalized bacteria revealed that the negative charge of bacteria decreases upon functionalization. As an example, Table S1 (Supporting Information) shows that the zeta potential of *E. coli* was reduced from −51.6 mV to −30.6 mV upon exposure to a 2 mM **IL-1a** and gold chloride solution. Similar results were obtained for **IL-1b**.

Galvanic Displacement Reaction and the Formation of a Luminescent Nanoshell on the Bacterial Surface. Here, antibodies act as a bridge for the electron transfer from gold to GaAs. As the antibodies have various functional groups, such as $-NH_2$, $-COOH$, $-CONH_2$, etc., they will interact with gold ions from the surface of bacteria and transport them toward the surface of GaAs. Subsequently, electron transfer takes place through the galvanic reaction involving the transfer of electrons from GaAs to metal ions, such as Au^{3+}, Ag^{+}, Rh^{3+}, and Pt^{2+}, that have relatively large redox potentials.[60] Buriak et al. have studied the formation of Au nanoparticles on the surface of GaAs through the electron transfer process,[61] and they have also characterized the formation of the Ga_xAu_y alloy at the interface of a Au nanoparticle and the GaAs substrate. The redox potential of the gold tripositive ion indicates its high tendency to gain an electron, whereas the negative potential of Ga metal indicates its affinity to lose electrons and become oxidized.[62,63]

The net positive potential of GDR between GaAs and gold ions (see Figure S1 for a schematics of the electron transfer reaction between the GaAs substrate and gold ions) makes this reaction spontaneous without the need of an external reducing agent.[64] It has been argued that the GaAs substrate could be coated with uniformly distributed Au nanoparticles.[65] To

DOI: 10.1021/acsabm.9b00932
ACS Appl. Bio Mater. 2020, 3, 477−485

investigate the formation of Au nanoparticles in our experiment, the GaAs substrate was functionalized with 1-hexadecanethiol (HDT) SAM using the reported method.[66] The HDT SAM-functionalized GaAs samples were treated with 100 μM solution of $AuCl_3$, which resulted in a uniform distribution of Au nanoparticles on the surface of the semiconductor as shown in Figure 3a. Consistent with this result is also a uniform distribution of *E. coli* bacteria decorated with metallic gold and immobilized on the biofunctionalized surface of GaAs as shown in Figure 3b.

An XPS spectrum of the GaAs surface exposed to a gold chloride solution for 30 min is shown in Figure 3c. The peaks at 84.01 and 84.84 eV, respectively, correspond to the Au $f_{7/2}$ electron of gold nanoparticles and Au_9Ga_4 alloy. This suggests the formation of gold−gallium alloy nanoparticles (Au_9Ga_4).[19,61] The peak at 83.7 eV, observed in Figure 3d, corresponds to the XPS Au 4f peak from GaAs functionalized with the HDT SAM and exposed to gold-coated bacteria. The energy of this peak was reduced in comparison to that of the gold nanoparticles (84.01 eV). It is reasonable to explain this shift on the basis of binding of nanogold with the bacterial membrane, which will reduce the binding strength of the metallic bond. Consequently, the kinetic energy of the respective electron will decrease.

Figure 4 shows optical microscopy images of green fluorescent protein (GFP) *E. coli* coated with Au nanoparticles

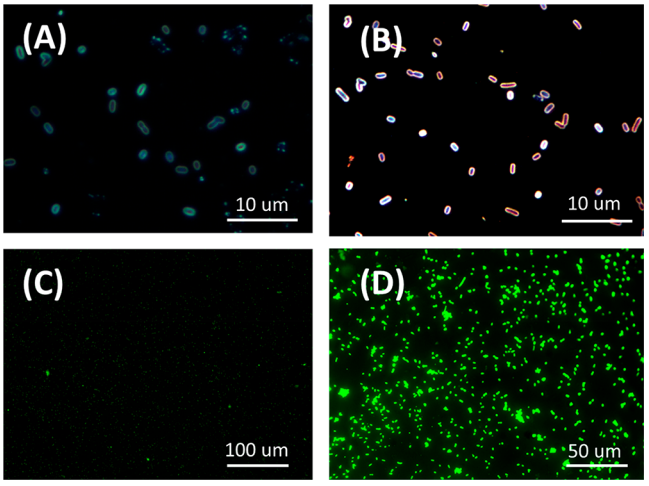

Figure 4. (a) Optical microscopy image of GFP *E. coli* (10^6 CFU/mL) on the surface of functionalized GaAs. (b) Optical microscopy image of Au^{3+}-coated GFP *E. coli* (10^6 CFU/mL) on the surface of functionalized GaAs. (c) Fluorescence microscopy image of gold ion coated GFP *E. coli* (10^8 CFU/mL) at an excitation wavelength of 473 nm. (d) Fluorescence microscopy image of gold ion coated GFP *E. coli* (10^8 CFU/mL) at an excitation wavelength of 377 nm.

by using an ionic liquid and excited with different photon energies. The biofunctionalized biochip was incubated for 1 h in a solution of GFP *E. coli* at 10^8 CFU/mL. The optical image of uncoated (Figure 4a) and Au^{3+}-coated (Figure 4b) bacteria can be easily distinguished, as the color of coated bacteria changes and the image becomes more intense. The bacteria appear more shiny, and their contours are better defined due to high reflectivity of gold metal ions. These data, supported by XPS analysis, are consistent with the formation of a thin shell of gold nanoparticles around the bacterial cell membrane, as further confirmed by fluorescence microscopy analysis shown in Figures 4(c) and 4(d). Normally, the GFP *E. coli* can be visualized by fluorescence microscopy upon excitation at 473 nm; however, in the case of gold-coated GFP *E. coli*, no fluorescence was observed due to the screening by the gold nanoshell (Figure 4c). In contrast, upon excitation at 377 nm, which corresponds to plasmonic absorption of gold,[67] a clear image of bacteria could be observed (Figure 4d).

Similar results were also observed for gold nanoshell decorated *L. pneumophila* immobilized with specific antibodies on the surface of GaAs. The optical microscopy images presented in Figure 5 show sharp contours of the coated

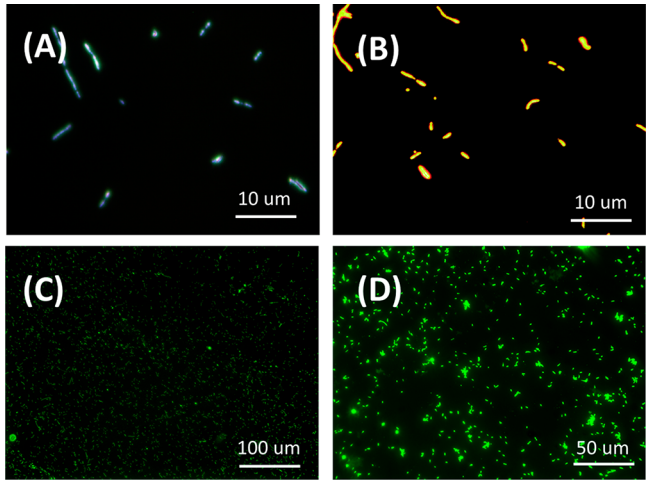

Figure 5. (a) Optical microscopy image of *L. pneumophila* (10^6 CFU/mL) on the surface of functionalized GaAs. (b) Optical microscopy image of Au^{3+}-coated *L. pneumophila* (10^6 CFU/mL) on the surface of functionalized GaAs. (c) Fluorescence microscopy image of gold ion coated *L. pneumophila* (10^8 CFU/mL) at an excitation wavelength of 473 nm. (d) Fluorescence microscopy image of gold ion coated *L. pneumophila* (10^8 CFU/mL) at an excitation wavelength of 377 nm.

bacteria (Figure 5b) in comparison to those recorded for the uncoated bacteria (Figure 5a), which illustrates the clear advantage of working with Au-coated *L. pneumophila*.

The capture of both uncoated and Au-coated *E. coli* and *L. pneumophila* bacteria was investiagted with Ab-functionalized GaAs biochips. No significant difference was observed in the absorption performance of antibodies for uncoated and Au-coated bacteria at 10^6 CFU/mL (Figure S2) and 10^5 CFU/mL (Figure S3). This suggests that Biginelli receptors with two binding units (positively charged cation for phosphate ion and thiourea subgroup for gold conjugation) provide an efficient interface for decorating bacteria with Au nanoparticles, while negligibly affecting the capture of bacteria by Abs. It should be noticed that the size of a gold ion is less than 99 pm,[68,69] which suggests that for a low surface coverage the footprint of all Au nanoparticles is significantly smaller than the surface area of a bacterium. The effect of pH on fluorescence imaging has also been examined, revealing that at an acidic pH = 4 the absorption of ionic liquids and ionic gold was significantly weaker than at pH = 7.4. A possible reason for this behavior is the protonation of phosphate ions on the bacterial cell membrane, which leads to a weaker interaction between the phosphate and imidazolium ionic liquid. Under such conditions, the interaction between antibody and bacteria would be significantly reduced.

DOI: 10.1021/acsabm.9b00932
ACS Appl. Bio Mater. 2020, 3, 477−485

The surface morphology of uncoated and ionic gold coated *E. coli* bacteria is illustrated with SEM images shown in Figure 6. While the uncoated bacteria reveal some features related to their surface structure,[70] the ionic gold exposed bacterium demonstrates the formation of a relatively continuous layer of Au and probably a Au_9Ga_4 alloy as suggested by the XPS spectra (Figure 3d). It should be mentioned that the formation of a Au/Au_9Ga_4 alloy layer on the bacterial surface through the galvanic displacement reaction takes place after bacteria had been immobilized with antibodies.

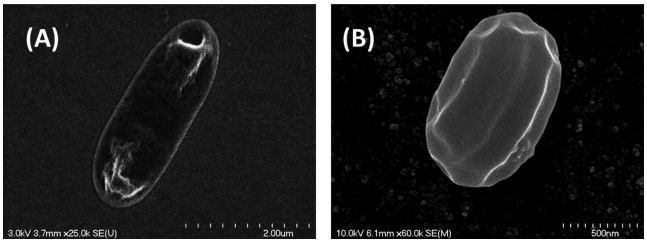

Figure 6. (a) Scanning electron microscopy image of *E. coli* bacteria incubated on the GaAs surface. (b) Gold ion (2 mM) coated *E. coli* showing the formation of a thin layer of metallic Au/Au_9Ga_4 alloy on the surface.

The change in hydrophilicity of the GaAs surface, upon treatment with gold ions and gold-coated bacteria, has been illustrated in Figure 7 with the contact angle measurements.

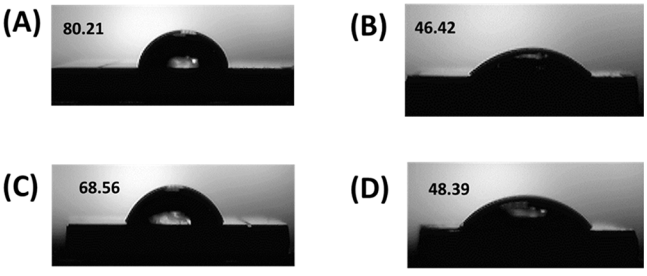

Figure 7. Contact angle measurement of the GaAs substrate (a) functionalized with HDT; (b) functionalized with HDT after treatment with gold chloride for 5 min; (c) coated with *E. coli* following the exposure to a bacterial suspension at 10^8 CFU/mL, and (d) coated with gold-decorated *E. coli* following the exposure to a bacterial suspension at 10^8 CFU/mL.

The results indicate the increase of hydrophilicity of the surface after gold treatment. Due to coverage with gold ions, the surface becomes rougher and more hydrophilic due to the hydration tendency of metallic gold and gold gallium alloy. The contact angle of the functionalized GaAs substrate decreased not only with deposition of gold nanoparticles but also with gold-coated bacteria.

CONCLUSIONS

We have demonstrated an innovative strategy for high-contrast imaging of bacteria. The surfaces of *L. pneumophila* and *E. coli* bacteria were coated with photoresponsive Au nanoparticles and Au_9Ga_4 alloy through the galvanic displacement reaction. In this approach, nanoparticles are formed by the spontaneous electron transfer between Au^{3+} ions and GaAs. The major advantage of the current procedure includes easy sample preparation, specific capture of a particular bacteria, and high-contrast imaging. The method does not require staining of bacteria with organic dye or conjugation with green fluorescent proteins. Therefore, the current approach has the potential to open a new window of opportunities in the field of bioimaging and biosensor devices.

EXPERIMENTAL SECTION

GaAs Substrate. The GaAs wafer used in this study was purchased from Azastra Inc. (Ottawa, Canada). Before dicing, the upper surface of the semiconductor wafers was protected with spin-coated photoresist.

Reagents. Biotinylated PEG thiols were purchased from Prochimia Surfaces (Sopot, Poland). All other thiols and phosphate-buffered saline (PBS) solution were purchased from Sigma Aldrich (Oakville, Canada). Organic reagents 2-hydroxybenzaldehyde, 4-hydroxybenzaldehyde, dibromoethane, urea, thiourea, ethyl-acetoacetate, and 1-methylimidazole were bought from Sigma Aldrich and used without further purification. Deionized water (18.2 MΩ) was used throughout the experiments. Acetonitrile and deuterated solvents were purchased from Merck and Sigma Aldrich, respectively. Semiconductor grade OptiClear (National Diagnostics), acetone (ACP Chemicals, Canada), isopropyl alcohol, and 28% ammonium hydroxide (Anachemia, Canada) were used without further purification.

Characterization. *a.1. X-ray Photoelectron Spectroscopy.* X-ray photoelectron spectroscopy (XPS) measurements were conducted in the Au 4f and Ga 4p region to investigate the chemical composition of the GaAs substrate after galvanic displacement reaction. The measurements were carried out with a Kratos Analytical AXIS Ultra DLD XPS spectrometer equipped with an Al Kα source operating at 150 W. For each measurement, the data were collected for a takeoff angle of 60° with respect to the surface normal.

b.1. FTIR Analysis. The binding of thiols on the GaAs surface was analyzed using the Fourier-transform infrared spectroscopy technique. The spectra were recorded in an absorbance mode using a Bruker Optics Hyperion 2000 FTIR system. The characteristic peak of the CH_2 stretching was analyzed for confirmation of thiolation. The samples washed with a series of organic solvents, followed by etching with ammonium hydroxide, were used as a reference.

c.1. Field Effect Scanning Electron Microscopy. The biofunctionalized biochip was exposed to bacterial (uncoated and gold coated) suspension at 10^6 CFU/mL for 1 hour, followed by washing with DI water. The surface morphology of bacteria (uncoated and Au/Au_9Ga_4 coated) was analyzed using a high-resolution scanning electron microscope (Zeiss LEO Supra 55 VP).

d.1. Contact Angle Measurements. The hydrophilicity of the GaAs substrate was analyzed using a contact angle measurement station (KRÜSS DSA30) composed of a visualization camera and a syringe of 10 μL volume. The ImageJ software was used to calculate the exact value of contact angle that is directly related to the hydrophilicity of the biosensor.

e.1. NMR Spectroscopy. The ^{1}H NMR and ^{13}C NMR spectra were recorded on a JEOL Instrument working at 400 MHz for ^{1}H NMR and at 100 MHz for ^{13}C NMR. All chemical shifts were recorded in ppm relative to tetramethylsilane as an internal reference (Figures S5−S19).

f.1. Optical Microscopy. The functionalized GaAs samples were analyzed with a ZEISS optical microscope with the total magnification of 500× working in DIC mode and DC mode. To record the optical microscopy images, the biofunctionalized biochip (10^6 CFU/mL) was exposed to bacteria for 1 h.

g.1. Fluorescence Microscopy. The presence of bacteria on the surface of biochips was analyzed using fluorescence microscopy. The green fluorescent protein (GFP) filters (excitation filter 473 nm/emission filter 520 nm) were used for GFP bacteria, and the DAP filters (excitation filter 377 nm/emission filter 447 nm) were used for gold-coated GFP bacteria. The biofunctionalized biochips were exposed to bacterial suspension at 10^8 CFU/mL for 1 h.

h.1. Zeta Potential Measurements. The bacteria were coated with ionic liquid and gold ion as described in the Experimental Section and

DOI: 10.1021/acsabm.9b00932
ACS Appl. Bio Mater. 2020, 3, 477−485

diluted to 10^6 CFU/mL concentration. The zeta potential of 10^6 CFU/mL of bacteria has been measured using a particle analyzer instrument from Metrohm.

Synthesis of Compound 2a. 4-Hydroxy-1-benzaldehyde (500 mg, 4.09 mmol), activated K_2CO_3, dibromoethane (3.5 mL, 40.9 mmol), and a pinch of tetrabutyl ammonium chloride (0.1 mmol) were dissolved in dry acetonitrile (25 mL), and the mixture was refluxed for 8 h. The progress of the reaction was monitored by using thin-layer chromatography (TLC). After completion of the reaction, the mixture was filtered, and the filtrate was evaporated under vacuum. Upon cooling the mixture at low temperature, a yellow solid compound **2a** was obtained with 90% yield. ^{1}H NMR (400 MHz, $CDCl_3$, ppm) δ 9.87 (s, 1H), 7.83 (dd, 2H), 6.99 (dd, 2H), 4.35 (t, 2H, J = 8 Hz), 3.65 (t, 2H, J = 4 Hz).^{13}C NMR (100 MHz, $CDCl_3$) δ: 190.3, 163.1, 132.2, 130.5, 114.9, 68.0, 28.6. ESI-MS (m/z) calcd 227.98, found: 229.15 [M + 2].

Synthesis of Compound 2b. The compound **2b** was synthesized using the same method as **1a**. 2-Hydroxy-1-benzaldehyde (500 mg, 4.09 mmol) was used instead of 4-hydroxy-1-benzaldehyde. ^{1}H NMR (400 MHz, $CDCl_3$, ppm) δ: 10.53 (s, 1H), 7.85 (d, 1H, J = 4 Hz), 7.54 (t, 1H, J = 8 Hz), 7.06 (t, 1H, J = 8 Hz), 6.95 (d, 1H, J = 8 Hz), 4.41 (t, 2H, J = 8 Hz), 3.70 (t, 2H, J = 8 Hz). ^{13}C NMR (100 MHz, $CDCl_3$) δ: 190.5, 159.2, 131.9, 130.3, 114.5, 68.5, 29.0. ESI-MS (m/z) calcd 227.98, found: 229.20 [M + 2].

Synthesis of Compound 3a. 4-(2-Bromoethoxy) benzaldehyde **2a** (50 mg, 0.40 mmol), urea (45.6 mg, 0.6 mmol), and ethyl acetoacetate (78.0 mg, 0.6 mmol) were dissolved in methanol with 2−3 drops of acetic acid added. The reaction mixture was refluxed for 12−14 h. The progress of the reaction mixture was monitored by TLC. The final product was isolated by silica gel column chromatography ($CHCl_3$-MeOH). ^{1}H NMR (400 MHz, DMSO d_6, ppm): δ: 8.91 (s, 1H), 8.25 (s, 1H), 7.25−7.23 (d, 2H, Ar−H, J = 8 Hz), 6.87−6.86 (d, 2H, Ar−H, J = 4 Hz), 5.50 (s, 1H, Ar−H), 4.34−4.31 (t, 2H, Ar−H, J = 4 Hz), 4.07−4.05 (q, 2H), 3.67−3.65 (t, 2H, J = 4 Hz), 2.30 (s, 3H), 1.29−1.25 (t, 3H, J = 8 Hz). ^{13}C NMR (100 MHz, DMSO-d_6) δ: 175.6, 165.5, 160.1, 158.1, 130.2, 125.1, 114.6, 103.3, 68.8, 61.2, 58.6, 30.3, 17.0, 12.6. Yield: 48%; white solid. ESI-MS (m/z) calcd 398.03, found: 398.18.

Synthesis of Compound 3b. 4-(2-Bromoethoxy) benzaldehyde **2b** (50 mg, 0.40 mmol), urea (45.6 mg, 0.6 mmol), and ethyl acetoacetate (78.0 mg, 0.6 mmol) were dissolved in methanol with 2−3 drops of acetic acid added. The reaction mixture was refluxed for 12−14 h. The progress of the reaction mixture was monitored by TLC. The final product was isolated by silica gel column chromatography ($CHCl_3$-MeOH). ^{1}H NMR (400 MHz, DMSO-d_6, ppm) δ: 8.79 (s, 1H), 8.40 (s, 1H), 7.48−7.46 (d, 1H, Ar−H, J = 8 Hz), 7.22−7.18 (m, 1H, Ar−H), 7.12−7.09 (m, 1H, Ar−H), 6.87−6.85 (dd, 1H, Ar−H, J = 8 Hz), 5.36 (s, 1H, Ar−H), 4.34−4.31 (t, 2H, J = 8 Hz), 4.07−4.05 (q, 2H), 3.67−3.65 (t, 2H, J = 4 Hz), 2.30 (s, 3H), 1.29−1.25 (t, 3H, J = 8 Hz). ^{13}C NMR (100 MHz, DMSO-d_6) δ: 175.6, 165.5, 160.1, 154.2, 130.2, 126.9, 122.1, 119.6, 111.4, 103.3, 68.8, 61.2, 56.6, 54.4, 17.0, 12.6. Yield: 48%; white solid. ESI-MS (m/z) calcd 398.03, found: 399.06 [M + 1].

Synthesis of Compound IL-1a. The compound **3a** (20 mg, 0.05 mmol) and 1-methylimidazole (4.92 mg, 0.06 mmol) were dissolved in an acetonitrile solvent, and the reaction mixture was refluxed for 10 h. The progress of the reaction was monitored by TLC. After the completion of the reaction, the solvent was removed under vacuum, and upon cooling, a white, solid compound was collected. The compound was washed two times with the acetonitrile solvent and dried well to get a final compound **IL-1a** in 40% yield. ^{1}H NMR (400 MHz, DMSO-d_6) δ: 9.10 (s, 1H), 8.75 (s, 1H), 7.98−7.92 (dd, 2H, Ar−H), 7.74−7.68 (dd, 2H, Ar−H), 7.34−7.28 (dd, 4H, Ar−H), 8.30 (s, 1H), 5.12 (s, 1H), 4.29−4.25 (t, 2H, J = 8 Hz), 4.16−4.10 (q, 2H), 3.77−3.73 (t, 2H, J = 8 Hz), 3.62 (s, 3H), 2.23 (s, 3H), 1.22 (t, 3H, J = 8 Hz).^{13}C NMR (100 MHz, DMSO-d_6) δ: 175.6, 165.5, 160.1, 158.1, 138.1, 130.2, 125.1, 123.7, 114.6, 103.3, 68.8, 61.2, 58.6, 54.4, 36.4, 17.0, 12.6. ESI-MS (m/z) calcd 401.16, found: 401.19.

Synthesis of Compound IL-1b. The compound **IL-1b** was synthesized using the same method as **IL-1a**; **3b** (20 mg, 0.05 mmol) was used instead of **3a**.^{1}H NMR (400 MHz, DMSO-d_6) δ: 9.10 (s, 1H), 8.75 (s, 1H), 8.30 (s, 1H), 7.78−7.72 (m, 2H, Ar−H), 7.34−7.28 (m, 2H, Ar−H), 6.64−6.58 (m, 2H, Ar−H), 5.12 (s, 1H), 4.29−4.25 (t, 2H, J = 8 Hz), 4.16−4.10 (q, 2H), 3.77−3.73 (t, 2H, J = 8 Hz), 3.62 (s, 3H), 2.23 (s, 3H), 1.14−1.10 (t, 3H, J = 8 Hz). ^{13}C NMR (100 MHz, DMSO-d_6) δ: 175.6, 165.5, 160.1, 154.2, 138.1, 130.2, 126.9, 123.7, 111.4, 103.3, 68.8, 61.2, 56.6, 54.4, 36.4, 17.0, and 12.6. Yield: 40%. ESI-MS (m/z) calcd 401.16, found: 401.35.

Functionalization of the GaAs Surface. *a.2. Washing.* The chips of 2 mm × 2 mm dimensions were cut from the GaAs wafer and sequentially cleaned with acetone, OptiClear, acetone, and isopropanol through 5 min sonication in each solvent. The cleaning of the sample was required to remove photoresist and some organic impurities from the surface. Further, the samples were treated with an ammonium hydroxide solution (28%) for two minutes to remove native oxides and, finally, washed with degassed ethanol.

b.2. Thiolation. To deposit a mixed thiol self-assembled monolayer (SAM) on the surface of GaAs substrate, the washed sample was incubated in a 1 mL solution of hexadecanethiol (HDT) (1.87 M) and PEG biotin thiol (0.13 M) in degassed ethanol for 20 h. The thiolated biochip was washed with ethanol to remove noncovalently attached thiol. However, to deposit the HDT SAM on the GaAs surface, the sample was incubated in 2 mM ethanoic solution of HDT for 20 h.

Note: The standard solution of thiols at a final concentration of 2 mM (1:15 PEG-biotin/HDT (M:M)) was prepared in degassed ethanol.

c.2. Neutravidin. GaAs samples were incubated in 200 μg/mL of neutravidin solution in PBS buffer for 2 h. The samples were washed with degassed PBS.

d.2. Biotinylated Antibody. To functionalize the surface with specific antibodies, the biochip was exposed to 0.4 mL of 100 μg/mL of PBS solution of biotinylated antibodies.

Functionalization of Bacteria. To functionalize the bacterial surface, *E. coli* suspended in PBS solution at 10^8 CFU/mL was exposed to a 2 mM solution of an imidazolium-based ionic liquid and the same concentration of gold chloride. The bacteria were kept in this mixture for 45 min, and subsequently, decorated bacteria were separated out through centrifugation. The separated bacteria were suspended in 1 mL of DI water and further diluted to achieve desired concentrations.

■ ASSOCIATED CONTENT

Supporting Information

The Supporting Information is available free of charge at https://pubs.acs.org/doi/10.1021/acsabm.9b00932.

> Graphical representation of electron transfer reaction, optical microscopy images of biofunctionalized and nonfunctionalized chips exposed to 10^6 CFU/mL of bacteria, zeta potential data, contact angle of GaAs coated with *L. pneumophila* bacteria at 10^8 CFU/mL, optical microscopy of GaAs with *E. coli*, and ^{1}H NMR and ^{13}C NMR mass spectra (PDF)

■ AUTHOR INFORMATION

Corresponding Authors

*Prof. Jan J. Dubowski. Email: jan.j.dubowski@usherbrooke.ca.
*Prof. Narinder Singh. Email: nsingh@iitrpr.ac.in.

ORCID

Narinder Singh: 0000-0002-8794-8157
Jan J. Dubowski: 0000-0003-0022-527X

Notes

The authors declare no competing financial interest.

DOI: 10.1021/acsabm.9b00932
ACS Appl. Bio Mater. 2020, 3, 477−485

■ ACKNOWLEDGMENTS

This work was supported by the Indo-Canada joint DBT/IC-IMPACTS research grant on *Portable Diagnostics and Analyzers* and the Natural Sciences and Engineering Research Council of Canada (NSERC) Strategic grant STPGP no. 494057. A.S. is thankful to FRQNT (Québec, Canada) for the support in the frame of the Merit Scholarship Program for Foreign Students (PBEEE).

■ REFERENCES

(1) Willets, K. A.; Wilson, A. J.; Sundaresan, V.; Joshi, P. B. Super-resolution imaging and plasmonics. *Chem. Rev.* **2017**, *117* (11), 7538−7582.

(2) Hu, L.; Wang, H.; Xia, T.; Fang, B.; Shen, Y.; Zhang, Q.; Tian, X.; Zhou, H.; Wu, J.; Tian, Y. Two-Photon-Active Organotin (IV) Complexes for Antibacterial Function and Superresolution Bacteria Imaging. *Inorg. Chem.* **2018**, *57* (11), 6340−6348.

(3) Vangara, A.; Pramanik, A.; Gao, Y.; Gates, K.; Begum, S.; Chandra Ray, P. Fluorescence resonance energy transfer based highly efficient theranostic nanoplatform for two-photon bioimaging and two-photon excited photodynamic therapy of multiple drug resistance bacteria. *ACS Applied Bio Materials* **2018**, *1* (2), 298−309.

(4) Wang, L.; Zhao, Q.; Zhang, Z.; Lu, Z.; Zhao, Y.; Tang, Y. Fluorescent Conjugated Polymer/Quarternary Ammonium Salt Co-assembly Nanoparticles: Applications in Highly Effective Antibacteria and Bioimaging. *ACS Applied Bio Materials* **2018**, *1* (5), 1478−1486.

(5) Lim, N. Y.; Ahn, J.; Won, M.; Choi, W.; Kim, J. S.; Jung, J. H. Novel Cyanostilbene-Based Fluorescent Chemoprobe for Hydroxyl Radicals and Its Two-Photon Bioimaging in Living Cells. *ACS Applied Bio Materials* **2019**, *2* (2), 936−942.

(6) Chan, H. L.; Lyu, L.; Aw, J.; Zhang, W.; Li, J.; Yang, H.-H.; Hayashi, H.; Chiba, S.; Xing, B. Unique fluorescent imaging probe for bacterial surface localization and resistant enzyme imaging. *ACS Chem. Biol.* **2018**, *13* (7), 1890−1896.

(7) Liu, G.-j.; Tian, S.-n.; Li, C.-y.; Xing, G.-w.; Zhou, L. Aggregation-Induced-Emission Materials with Different Electric Charges as an Artificial Tongue: Design, Construction, and Assembly with Various Pathogenic Bacteria for Effective Bacterial Imaging and Discrimination. *ACS Appl. Mater. Interfaces* **2017**, *9* (34), 28331−28338.

(8) Mukherji, R.; Samanta, A.; Illathvalappil, R.; Chowdhury, S.; Prabhune, A.; Devi, R. N. Selective imaging of quorum sensing receptors in bacteria using fluorescent Au nanocluster probes surface functionalized with signal molecules. *ACS Appl. Mater. Interfaces* **2013**, *5* (24), 13076−13081.

(9) Bari, N. K.; Kumar, G.; Bhatt, A.; Hazra, J. P.; Garg, A.; Ali, M. E.; Sinha, S. Nanoparticle fabrication on bacterial microcompartment surface for the development of hybrid enzyme-inorganic catalyst. *ACS Catal.* **2018**, *8* (9), 7742−7748.

(10) Xu, X.; Chen, Y.; Wei, H.; Xia, B.; Liu, F.; Li, N. Counting bacteria using functionalized gold nanoparticles as the light-scattering reporter. *Anal. Chem.* **2012**, *84* (22), 9721−9728.

(11) Verma, M. S.; Rogowski, J. L.; Jones, L.; Gu, F. X. Colorimetric biosensing of pathogens using gold nanoparticles. *Biotechnol. Adv.* **2015**, *33* (6), 666−680.

(12) Huerta-Aguilar, C. A.; Ramirez-Guzman, B.; Thangarasu, P.; Narayanan, J.; Singh, N. Simultaneous recognition of cysteine and cytosine using thiophene-based organic nanoparticles decorated with Au NPs and bio-imaging of cells. *Photochemical & photobiological sciences: Official journal of the European Photochemistry Association and the European Society for Photobiology* **2019**, *18* (7), 1761−1772.

(13) Sidhu, J. S.; Mayank; Pandiyan, T.; Kaur, N.; Singh, N. The Photochemical Degradation of Bacterial Cell Wall Using Penicillin-Based Carbon Dots: Weapons Against Multi-Drug Resistant (MDR) Strains. *ChemistrySelect* **2017**, *2* (29), 9277−9283.

(14) Liu, R.; Sen, A. Unified synthetic approach to silver nanostructures by galvanic displacement reaction on copper: from nanobelts to nanoshells. *Chem. Mater.* **2012**, *24* (1), 48−54.

(15) Messina, M. M.; Picone, A. L.; dos Santos Claro, P. C.; Ruiz, R.; Saccone, F. D.; Romano, R. M.; Ibanez, F. J. Graphene Grown on Ni Foam: Molecular Sensing, Graphene-Enhanced Raman Scattering, and Galvanic Exchange for Surface-Enhanced Raman Scattering Applications. *J. Phys. Chem. C* **2018**, *122* (16), 9152−9161.

(16) Miyazaki, M.; Furukawa, S.; Takayama, T.; Yamazoe, S.; Komatsu, T. Surface Modification of PdZn Nanoparticles via Galvanic Replacement for the Selective Hydrogenation of Terminal Alkynes. *ACS Applied Nano Materials* **2019**, *2* (5), 3307−3314.

(17) Rao, C.; Luber, E. J.; Olsen, B.; Buriak, J. M. Plasmonic Stamps Fabricated by Gold Dewetting on PDMS for Catalyzing Hydrosilylation on Silicon Surfaces. *ACS Applied Nano Materials* **2019**, *2* (5), 3238−3245.

(18) Lindley, S. A.; Zhang, J. Z. Bumpy Hollow Gold Nanospheres for Theranostic Applications: Effect of Surface Morphology on Photothermal Conversion Efficiency. *ACS Applied Nano Materials* **2019**, *2* (2), 1072−1081.

(19) Sayed, S. Y.; Buriak, J. M. Epitaxial growth of nanostructured gold films on germanium via galvanic displacement. *ACS Appl. Mater. Interfaces* **2010**, *2* (12), 3515−3524.

(20) Song, B.; He, K.; Yuan, Y.; Sharifi-Asl, S.; Cheng, M.; Lu, J.; Saidi, W. A.; Shahbazian-Yassar, R. In situ study of nucleation and growth dynamics of Au nanoparticles on MoS 2 nanoflakes. *Nanoscale* **2018**, *10* (33), 15809−15818.

(21) Sun, Y.; Lei, C.; Gosztola, D.; Haasch, R. Formation of oxides and their role in the growth of Ag nanoplates on GaAs substrates. *Langmuir* **2008**, *24* (20), 11928−11934.

(22) Sun, Y. Growth of silver nanowires on GaAs wafers. *Nanoscale* **2011**, *3* (5), 2247−2255.

(23) Zhang, C.; Luo, L.; Luo, J.; Evans, D. G.; Sun, X. A process-analysis microsystem based on density gradient centrifugation and its application in the study of the galvanic replacement mechanism of Ag nanoplates with $HAuCl_4$. *Chem. Commun.* **2012**, *48* (58), 7241−7243.

(24) Kim, S.-J.; Seong, M.; Yun, H.-W.; Ahn, J.; Lee, H.; Oh, S. J.; Hong, S.-H. Chemically Engineered Au-Ag Plasmonic Nanostructures to Realize Large Area and Flexible Metamaterials. *ACS Appl. Mater. Interfaces* **2018**, *10* (30), 25652−25659.

(25) Kim, T.; Fu, X.; Warther, D.; Sailor, M. J. Size-controlled Pd nanoparticle catalysts prepared by galvanic displacement into a porous Si-Iron oxide nanoparticle host. *ACS Nano* **2017**, *11* (3), 2773−2784.

(26) Porter, L. A.; Choi, H. C.; Ribbe, A. E.; Buriak, J. M. Controlled electroless deposition of noble metal nanoparticle films on germanium surfaces. *Nano Lett.* **2002**, *2* (10), 1067−1071.

(27) Aizawa, M.; Buriak, J. M. Block copolymer-templated chemistry on Si, Ge, InP, and GaAs surfaces. *J. Am. Chem. Soc.* **2005**, *127* (25), 8932−8933.

(28) Nazemi, E.; Aithal, S.; Hassen, W. M.; Frost, E. H.; Dubowski, J. J. GaAs/AlGaAs heterostructure based photonic biosensor for rapid detection of Escherichia coli in phosphate buffered saline solution. *Sens. Actuators, B* **2015**, *207*, 556−562.

(29) Nazemi, E.; Hassen, W. M.; Frost, E. H.; Dubowski, J. J. Monitoring growth and antibiotic susceptibility of Escherichia coli with photoluminescence of GaAs/AlGaAs quantum well microstructures. *Biosens. Bioelectron.* **2017**, *93*, 234−240.

(30) Aziziyan, M. R.; Hassen, W. M.; Morris, D.; Frost, E. H.; Dubowski, J. J. Photonic biosensor based on photocorrosion of GaAs/AlGaAs quantum heterostructures for detection of Legionella pneumophila. *Biointerphases* **2016**, *11* (1), 019301.

(31) Hassen, W. M.; Sanyal, H.; Hammood, M.; Moumanis, K.; Frost, E. H.; Dubowski, J. J. Chemotaxis for enhanced immobilization of Escherichia coli and Legionella pneumophila on biofunctionalized surfaces of GaAs. *Biointerphases* **2016**, *11* (2), 021004.

(32) Aziziyan, M. R.; Hassen, W. M.; Sharma, H.; Shirzaei Sani, E.; Annabi, N.; Frost, E. H.; Dubowski, J. J. Sodium Dodecyl Sulfate Decorated Legionella pneumophila for Enhanced Detection with a GaAs/AlGaAs Nanoheterostructure Biosensor. *Sens. Actuators, B* **2020**, *304*, 127007.

(33) Sharma, H.; Sidhu, J. S.; Hassen, W. M.; Singh, N.; Dubowski, J. J. Synthesis of a 3,4-Disubstituted 1,8-Naphthalimide-Based DNA

DOI: 10.1021/acsabm.9b00932
ACS Appl. Bio Mater. 2020, 3, 477−485

Intercalator for Direct Imaging of Legionella pneumophila. *ACS Omega* **2019**, *4* (3), 5829−5838.
(34) Fields, B. S.; Benson, R. F.; Besser, R. E. Legionella and Legionnaires' disease: 25 years of investigation. *Clin. Microbiol. Rev.* **2002**, *15* (3), 506−526.
(35) Diederen, B. M. W. Legionella spp. and Legionnaires' disease. *J. Infect.* **2008**, *56* (1), 1−12.
(36) MacIntyre, C. R.; Dyda, A.; Bui, C. M.; Chughtai, A. A. Rolling epidemic of Legionnaires disease outbreaks in small geographic areas. *Emerging Microbes Infect.* **2018**, *7* (1), 1−10.
(37) Zheng, Z.; Guo, J.; Mao, H.; Xu, Q.; Qin, J.; Yan, F. Metal-containing poly (ionic liquid) membranes for antibacterial applications. *ACS Biomater. Sci. Eng.* **2017**, *3* (6), 922−928.
(38) Zheng, Z.; Xu, Q.; Guo, J.; Qin, J.; Mao, H.; Wang, B.; Yan, F. Structure-antibacterial activity relationships of imidazolium-type ionic liquid monomers, poly (ionic liquids) and poly (ionic liquid) membranes: effect of alkyl chain length and cations. *ACS Appl. Mater. Interfaces* **2016**, *8* (20), 12684−12692.
(39) Bhattacharya, G.; Giri, R.; Saxena, H.; Agrawal, V.; Gupta, A.; Mukhopadhyay, M.; Ghosh, S. X-ray reflectivity study of the interaction of an imidazolium-based ionic liquid with a soft supported lipid membrane. *Langmuir* **2017**, *33* (5), 1295−1304.
(40) Aditya, A.; Chattopadhyay, S.; Jha, D.; Gautam, H. K.; Maiti, S.; Ganguli, M. Zinc oxide nanoparticles dispersed in ionic liquids show high antimicrobial efficacy to skin-specific bacteria. *ACS Appl. Mater. Interfaces* **2018**, *10* (18), 15401−15411.
(41) Soni, S. K.; Sarkar, S.; Mirzadeh, N.; Selvakannan, P.; Bhargava, S. K. Self-assembled functional nanostructure of plasmid DNA with ionic liquid [Bmim][PF6]: enhanced efficiency in bacterial gene transformation. *Langmuir* **2015**, *31* (16), 4722−4732.
(42) Singh, A.; Raj, P.; Singh, N. Benzimidazolium-based self-assembled fluorescent aggregates for sensing and catalytic degradation of diethylchlorophosphate. *ACS Appl. Mater. Interfaces* **2016**, *8* (42), 28641−28651.
(43) Ventura, S. n. P.; Gurbisz, M.; Ghavre, M.; Ferreira, F. b. M.; Goncalves, F.; Beadham, I.; Quilty, B.; Coutinho, J. A.; Gathergood, N. Imidazolium and pyridinium ionic liquids from mandelic acid derivatives: Synthesis and bacteria and algae toxicity evaluation. *ACS Sustainable Chem. Eng.* **2013**, *1* (4), 393−402.
(44) Singh, A.; Raj, P.; Singh, A.; Dubowski, J. J.; Kaur, N.; Singh, N. Metal−Organocatalyst for Detoxification of Phosphorothioate Pesticides: Demonstration of Acetylcholine Esterase Activity. *Inorg. Chem.* **2019**, *58* (15), 9773−9784.
(45) Chen, Z.; Yuan, H.; Liang, H. Synthesis of multifunctional cationic poly (p-phenylenevinylene) for selectively killing bacteria and lysosome-specific imaging. *ACS Appl. Mater. Interfaces* **2017**, *9* (11), 9260−9264.
(46) Huang, Y.; Pappas, H. C.; Zhang, L.; Wang, S.; Cai, R.; Tan, W.; Wang, S.; Whitten, D. G.; Schanze, K. S. Selective imaging and inactivation of bacteria over mammalian cells by imidazolium-substituted polythiophene. *Chem. Mater.* **2017**, *29* (15), 6389−6395.
(47) Zhu, J.-H.; Yu, C.; Chen, Y.; Shin, J.; Cao, Q.-Y.; Kim, J. S. A self-assembled amphiphilic imidazolium-based ATP probe. *Chem. Commun.* **2017**, *53* (31), 4342−4345.
(48) Yang, Y.; Wang, X.; Cui, Q.; Cao, Q.; Li, L. Self-assembly of fluorescent organic nanoparticles for iron (III) sensing and cellular imaging. *ACS Appl. Mater. Interfaces* **2016**, *8* (11), 7440−7448.
(49) Cui, Q.; Wang, X.; Yang, Y.; Li, S.; Li, L.; Wang, S. Binding-directed energy transfer of conjugated polymer materials for dual-color imaging of cell membrane. *Chem. Mater.* **2016**, *28* (13), 4661−4669.
(50) Cui, Q.; Yang, Y.; Yao, C.; Liu, R.; Li, L. Aggregation-Induced Energy Transfer of Conjugated Polymer Materials for ATP Sensing. *ACS Appl. Mater. Interfaces* **2016**, *8* (51), 35578−35586.
(51) Yan, K.; Lok, C.-N.; Bierla, K.; Che, C.-M. Gold (I) complex of N, N-disubstituted cyclic thiourea with in vitro and in vivo anticancer properties potent tight-binding inhibition of thioredoxin reductase. *Chem. Commun.* **2010**, *46* (41), 7691−7693.
(52) Schwade, V. D.; Kirsten, L.; Hagenbach, A.; Lang, E. S.; Abram, U. Indium (III), lead (II), gold (I) and copper (II) complexes with isophthaloylbis (thiourea) ligands. *Polyhedron* **2013**, *55*, 155−161.
(53) Nazemi, E.; Hassen, W. M.; Frost, E. H.; Dubowski, J. J. Growth of Escherichia coli on the GaAs (001) surface. *Talanta* **2018**, *178*, 69−77.
(54) Choinière, S.; Frost, E. H.; Dubowski, J. J. Binding strategies for capturing and growing Escherichia coli on surfaces of biosensing devices. *Talanta* **2019**, *192*, 270−277.
(55) Lacour, V.; Moumanis, K.; Hassen, W. M.; Elie-Caille, C.; Leblois, T.; Dubowski, J. J. Formation Kinetics of Mixed Self-Assembled Monolayers of Alkanethiols on GaAs(100). *Langmuir* **2019**, *35* (13), 4415−4427.
(56) Sharma, H.; Moumanis, K.; Dubowski, J. J. pH-Dependent Photocorrosion of GaAs/AlGaAs Quantum Well Microstructures. *J. Phys. Chem. C* **2016**, *120* (45), 26129−26137.
(57) Garcia, M. T.; Ribosa, I.; Perez, L.; Manresa, A.; Comelles, F. Aggregation behavior and antimicrobial activity of ester-functionalized imidazolium-and pyridinium-based ionic liquids in aqueous solution. *Langmuir* **2013**, *29* (8), 2536−2545.
(58) Parthasarathy, A.; Pappas, H. C.; Hill, E. H.; Huang, Y.; Whitten, D. G.; Schanze, K. S. Conjugated polyelectrolytes with imidazolium solubilizing groups. Properties and application to photodynamic inactivation of bacteria. *ACS Appl. Mater. Interfaces* **2015**, *7* (51), 28027−28034.
(59) Raj, T.; Sharma, H.; Singh, A.; Aree, T.; Kaur, N.; Singh, N.; Jang, D. O. Solvent-Less Mechanochemical Approach to the Synthesis of Pyrimidine Derivatives. *ACS Sustainable Chem. Eng.* **2017**, *5* (2), 1468−1475.
(60) Xia, X.; Wang, Y.; Ruditskiy, A.; Xia, Y. 25th Anniversary Article: Galvanic Replacement: A Simple and Versatile Route to Hollow Nanostructures with Tunable and Well-Controlled Properties. *Adv. Mater.* **2013**, *25* (44), 6313−6333.
(61) Sayed, S. Y.; Daly, B.; Buriak, J. M. Characterization of the Interface of Gold and Silver Nanostructures on InP and GaAs Synthesized via Galvanic Displacement. *J. Phys. Chem. C* **2008**, *112* (32), 12291−12298.
(62) Cotton, F. A.; Wilkinson, G. *Advanced inorganic chemistry*, 5th ed.; Wiley: New York, 1988; Vol. *6*, p xvii, 1455 p.
(63) Vanysek, P. Electrochemical Series. In *Handbook of Chemistry and Physics*; Chemical Rubber Company: Boca Raton, 2011.
(64) Magagnin, L.; Maboudian, R.; Carraro, C. Gold deposition by galvanic displacement on semiconductor surfaces: effect of substrate on adhesion. *J. Phys. Chem. B* **2002**, *106* (2), 401−407.
(65) Aizawa, M.; Buriak, J. M. Block copolymer templated chemistry for the formation of metallic nanoparticle arrays on semiconductor surfaces. *Chem. Mater.* **2007**, *19* (21), 5090−5101.
(66) Huang, X.; Dubowski, J. J. Solvent-mediated self-assembly of hexadecanethiol on GaAs (0 0 1). *Appl. Surf. Sci.* **2014**, *299*, 66−72.
(67) Chen, Y.; Wu, H.; Li, Z.; Wang, P.; Yang, L.; Fang, Y. The study of surface plasmon in Au/Ag core/shell compound nanoparticles. *Plasmonics* **2012**, *7* (3), 509−513.
(68) Burrows, J. A.; Pauling, L. The nature of the chemical bond and the structure of molecules aid crystals. Ithaca: The Cornell University Press, 1939. 430 p. *Sci. Educ.* **1941**, *25* (2), 120−120.
(69) Ahrens, L. H. The use of ionization potentials Part 1. Ionic radii of the elements. *Geochim. Cosmochim. Acta* **1952**, *2* (3), 155−169.
(70) Golding, C. G.; Lamboo, L. L.; Beniac, D. R.; Booth, T. F. The scanning electron microscope in microbiology and diagnosis of infectious disease. *Sci. Rep.* **2016**, *6*, 26516.

DOI: 10.1021/acsabm.9b00932
ACS Appl. Bio Mater. 2020, 3, 477−485